Superconductor Science and Technology

PAPER • OPEN ACCESS

A sulfurization method for creating the buffer-layers current flow diverter architecture in $REBa_2Cu_3O_7$ coated conductors

To cite this article: P Barusco *et al* 2023 *Supercond. Sci. Technol.* **36** 125005

View the article online for updates and enhancements.

You may also like

- *In vitro* investigation of an intracranial flow diverter with a fibrin-based, hemostasis mimicking, nanocoating
Antonia Link, Tatjana Michel, Martin Schaller et al.
- Concept of a current flow diverter for accelerating the normal zone propagation velocity in 2G HTS coated conductors
Christian Lacroix and Frederic Sirois
- Evaluation of hydrocarbon flow standard facility equipped with double-wing diverter using four types of working liquids
R Doihara, T Shimada, K H Cheong et al.

This content was downloaded from IP address 95.17.57.110 on 04/01/2024 at 18:53

OPEN ACCESS
IOP Publishing
Superconductor Science and Technology
Supercond. Sci. Technol. **36** (2023) 125005 (10pp)
https://doi.org/10.1088/1361-6668/ad01ec

A sulfurization method for creating the buffer-layers current flow diverter architecture in $REBa_2Cu_3O_7$ coated conductors

P Barusco[1,*], J Giguère[2], C Lacroix[2], F Sirois[2], X Granados[1], T Puig[1] and X Obradors[1,*]

[1] Institut de Ciència de Materials de Barcelona (ICMAB-CSIC), Campus de la UAB, 08193 Bellaterra, Catalonia, Spain
[2] Polytechnique Montréal, 2500 Chemin de Polytechnique, Montréal, QC H3T 1J4, Canada

E-mail: pebarusco@gmail.com and xavier.obradors@icmab.es

Received 9 June 2023, revised 25 September 2023
Accepted for publication 10 October 2023
Published 19 October 2023

Abstract

The current flow diverter (CFD) is a known concept that has proven to effectively reduce the probability of destructive hot spots in $REBa_2Cu_3O_7$ (REBCO; RE = rare earth) coated conductors (CCs) by boosting the normal zone propagation velocity. However, the implementation of the CFD concept requires additional steps in a fabrication process that is already complex and has struggled to find a simple reel-to-reel fabrication method. This work reports on the details of a fabrication route for the buffer-layers-CFD (bCFD) architecture using a solid-vapor silver sulfurization technique to tune the geometry of the metal stabilizer in the high-temperature superconductor tape. The analysis of the microstructure and superconducting properties of the Ag_2S/Ag/GdBCO trilayer processed under different conditions shows how we achieved a new customized functional CC with the bCFD architecture. In DC limitation experiments, this bCFD-sulfide architecture allowed to generate an electric potential much faster than the conventional architecture (60 V s^{-1} vs. 1.2 V s^{-1}) thanks to the strong enhancement of the NPZV.

Supplementary material for this article is available online

Keywords: normal zone propagation velocity (NZPV), current flow diverter (CFD), coated conductors (CC), HTS-tape, superconductivity

(Some figures may appear in colour only in the online journal)

* Authors to whom any correspondence should be addressed.

Original content from this work may be used under the terms of the Creative Commons Attribution 4.0 licence. Any further distribution of this work must maintain attribution to the author(s) and the title of the work, journal citation and DOI.

 © 2023 The Author(s). Published by IOP Publishing Ltd

1. Introduction

The second generation (2G) of high-temperature superconductor (HTS) tapes, i.e. coated conductors (CCs, also known as 'HTS-tapes'), is considered a prime candidate for improving performance in a wide range of superconducting electrical power devices, such as motors, generators, transmission cables and superconductor fault current limiters (SFCLs), as well as high-field magnets [1–7]. However, the 'hot spot' regime is a well-known inherent issue of the tape's architecture that hinders its reliable continuous operation. If by an unexpected event, the operating current fluctuates near the average critical current (I_c) of the conductor, zones with lower I_c [8] can locally (lengthwise) quench [9], i.e. they can switch from the superconducting state to the resistive normal state. Due to the low thermal conductivity (W/m-K) and high heat capacity (J/kg-K) of HTS tapes [10], these zones can become 'hot spots' given the slow thermal propagation of the local quench, also referred to as normal zone propagation velocity (NZPV) [11–13]. If the NZPV is slow (in the cm s^{-1} range) and the current in the conductor is not limited quickly enough, the local joule heating of the HTS resistive state in the hot spot is likely to irreversibly damage the tape [14], and even rupture the cross-section of the CC completely. Recently, an experimental study from Lacroix *et al* [15] comparing the NZPV at 77 K and self-field of different REBCO CC architectures mentioned a sulfurization technique capable of effectively creating the buffer-layers-CFD (bCFD) architecture (figure 1) which allowed to increase the NZPV by a factor of 18. In this paper, we describe this approach in further details.

In a typical CC architecture, a thin (<2 μm) continuous noble metal coating of silver is deposited on the REBCO layer for two main reasons: to protect it from atmospheric degradation [16], and to provide a low interfacial resistance (Ω cm^2) path for injecting current [17]. In the presence of a *hot spot*, this stabilizer coating also shunts the current from the quenched zone and reduces the joule heating. Consequently, the most common solution adopted by CC manufacturers against hot spots is to add an extra thick (>10 μm) metal shunt, i.e. copper, onto the noble metal stabilizer [18]. However, this method decreases the normal state resistance (Ω m^{-1}) of the final tape, thus making an SFCL significantly more expensive [19]. In the case of magnets and motors, a thicker shunt further increases the heat capacity and reduces the NZPV to the point of jeopardizing quench detection systems by delaying the proper interruption of the power source [20]. In addition, the thick shunt reduces the engineering critical current of the CC, resulting in a reduction of the maximum field intensity achievable by the magnet.

The current flow diverter (CFD) is a proven concept that deals with the *hot spot* scenario by significantly increasing the NZPV (at least one order of magnitude) without changing the final normal state resistance (Ω m^{-1}) of the CC [21, 22]. In the classic CFD concept, the architecture is implemented by increasing the interfacial resistance (Ω cm^2) Ag/REBCO solely in the middle of the CC's width along its length as shown in figures 1 and S1. Meanwhile, the global interfacial resistance Ag/REBCO across the width maintains a relatively low value ($\sim 10^{-7}$ Ω cm^2) to allow for proper current injection at the terminals. Although efficient, the main bottleneck for the reel-to-reel fabrication of traditional CFD-tapes is in how to create the high interfacial resistance Ag/REBCO without having to change substantially the already established fabrication process. For instance, the original proof-of-concept technique of silver etching and re-sputtering described in [23] is not economically attractive for the production of silver coated CCs in long lengths.

An industrially compatible method to produce CFD tapes was proposed for CCs from STI Inc. and was based on reactive co-evaporation and cyclic deposition reaction [24] of cerium oxide (CeO_2) as the CFD layer (Ag/CeO_2/REBCO). However, the CeO_2 showed significant reactivity with the REBCO at the interface, leading to a drastic degradation of the superconducting properties [25]. More recently, another low-cost method using the chemical solution deposition of amorphous yttrium oxide (Y_2O_3) was proposed to form a CFD trilayer Ag/Y_2O_3/REBCO on *THEVA GmbH* CCs. Although compatible with the REBCO layer, this yttria-CFD approach requires adding some extra steps to the traditional CC fabrication process [26].

Alternatively, the bCFD (or 'bCFD' in figure S1) introduced in [27], and tested in [28] as an extension of the CFD concept, uses the electrical insulation properties of the buffer layers already present in CCs. The bCFD increases the NZPV by modifying solely the thickness ratio between the top and bottom stabilizer layers. In the presence of a *hot spot*, having a thin (20–100 nm) silver stabilizer on top of the HTS and a thick layer on the bottom substrate side forces the current to divert around the insulating buffer layers towards the Hastelloy substrate and the bottom stabilizer, which provokes the desired NZPV boost. This approach is, in theory, much simpler than the classic CFD since it avoids having to alter the original interface Ag/REBCO in the tape. Nevertheless, one must find a way to keep a continuous thin silver thickness (<100 nm) as the top stabilizer layer on the final CC. This thickness requirement is the main challenge for the bCFD since thin silver layers (<100 nm) are known to aggregate and form discontinuous silver islands (i.e. dewetting) during heat treatments [29], like the final oxygen annealing process required for loading oxygen into the $REBa_2Cu_3O_{7-\delta}$ [30–32]. In [33], it has been shown that a 20 nm thick silver layer on top of YBCO forms spherical islands and becomes electrically discontinuous when annealed at temperatures as low as 300 °C. Therefore, the partial replacement of the Ag stabilizer with Ag_2S to tune the effective stabilizer thickness on silver coated commercial CCs, come as a cheap and simple solution for implementing the bCFD [15]. Furthermore, there already exists extensive experience in scaling up the sulfurization processes in the fabrication of large area copper indium gallium sulfur (CIGS) solar cells and thus it is expected that it should be also feasible for Ag_2S [34–36].

In this paper, the authors reveal how the silver was experimentally tested with two sulfurization processes on samples taken from a reel of commercial THEVA tape to find the optimal processing conditions. The effect of the final sulfide layer on the CC was evaluated via scanning electron

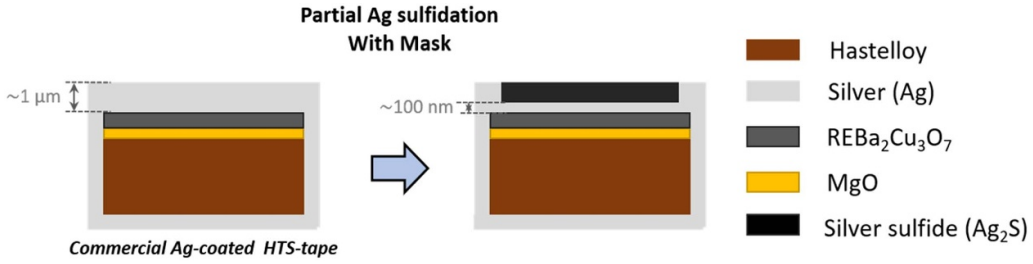

Figure 1. Schematic of the HTS-tape cross-section before and after the partial sulfurization process of the upper silver layer to create the bCFD-sulfide architecture.

microscopy (SEM)/focus ion beam (FIB) images, x-ray diffraction, scanning Hall probe microscopy (SHPM) and DC limitation tests.

2. Experimental method

All REBCO CC samples used as template came from a reel-to-reel manufacturing unit produced by THEVA [37]. The CC architecture consisted of a 100 μm thick electropolished Hastelloy substrate, on which a 3 μm thick texturized layer of MgO was evaporated using an inclined substrate deposition technique (ISD) [38, 39], and a second 450 nm thick coating of MgO was deposited at a perpendicular angle. Afterward, a 3 μm thick layer of GdBCO HTS was grown on top of the MgO via electron beam evaporation from a granulate [37, 40]. A 1–1.2 μm thick silver layer surrounds the whole tape.

The first sulfurization experiment was performed with a commercial solution of liver of sulfur gel traded under the name '*Liver of Sulfur Extended Gel (XL Gel)*', commonly used to create patina in jewel pieces. According to the manufacture's datasheet, the XL Gel is a mixture of potassium thiosulfate hydrated, potassium trisulfide and trade secret additives for extended shelf life. About 12 $\times$ 12 mm pieces of HTS-tape coated with 1–1.2 μm of surrounding silver were stuck onto a glass slide with polyimide tape and dipped into pre-heated solutions of XL Gel + distilled water with temperatures between 30 °C and 50 °C (figure 2(a)). This temperature range was chosen to avoid rapidly decomposing the liver of sulfur into potassium sulfate (K_2SO_4) and potassium carbonate (K_2CO_3), neither of which has an oxidizing effect on silver [41].

The second sulfurization experiment was performed using sublimed sulfur powder (−100 mesh 99.5%) from *Alfa Aesar* as a source of sulfur gas (S_n). Pure sulfur was chosen instead of H_2S due to the exothermic nature of its reaction with silver, thus requiring no extra heat to promote the sulfurization. Samples were positioned inside a hermetic glass jar of 500 ml together with a small petri dish containing 10 mg of the powder (figure 2(b)). To create the vapor pressure condition, the jar was heated on a hot-plate (IKA C-MAG HS 7) beyond the melting temperature of sulfur (115.21 °C at 1 atm) up to 130 °C, thus creating a sulfur pressure dominated by S_8 allotropes [42].

The x-ray diffraction patterns of the CFD CCs were obtained using a general area detector GADDS diffractometer (Bruker-AXS model D8) equipped with a 2D detector and operating with Cu Kα radiation. The surface morphology of the films was analyzed using SEM (SEM FEI Quanta 200 FEG) and the FIB cross-section images were acquired with a dual beam (SEM-FIB) Zeiss 1560 XB apparatus.

The superconducting properties in the GdBCO layer were evaluated with a homemade SHPM system [43]. Samples were field cooled at 77 K with liquid nitrogen, in the presence of a NdFeB permanent magnet large enough to cover the whole sample. After removing the permanent magnet, the samples remained in a self-field condition and then they were spatially scanned with a Hall-probe for obtaining a map of the distribution of the perpendicular trapped magnetic field B_z. Solving the inverse Fourier problem for B_z, we could estimate the distribution of the critical current density J_c, as well as the critical current I_c. The I_c was calculated by integrating J_c over a virtual closed path inside the samples considering the appropriate cross-section area, as described in [43].

The current limitation tests shown here were taken during the European H2020-FASTGRID project which goal was to develop the best 2G HTS CC architecture for a superconducting fault current limiter (FCL) operating in a DC electrical network [5]. Large tape samples ($\geqslant$12 cm) were tested in DC fault current conditions using a setup similar to the one described in [44]. A voltage source was connected to both ends of samples with copper blocks held by bolts and screws. A fast acquisition voltmeter monitored the global electric field across the sample using two gold-plated pogo-pins. During the limitation experiments, the sample was immersed in a liquid nitrogen bath in ambient conditions (77 K). Before and after the limitation tests, the critical current of the samples was measured to determine if degradation occurred during the limitation tests.

3. Results

3.1. Liver of sulfur reaction

Table 1 shows the decomposition time for XL Gel solutions with different concentrations depending on temperature. The state of the decomposition was identifiable by observing the solution's color fade from bright yellow to milky white. The 12 $\times$ 12 mm HTS tape samples were submerged in each solution and removed once the decomposition was complete (figure 2(a)).

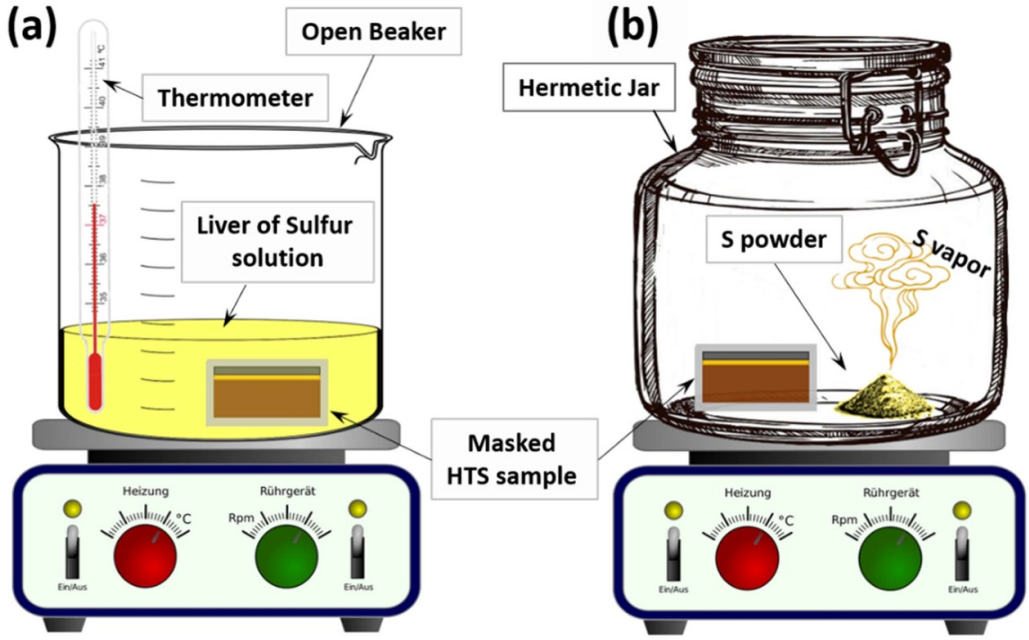

Figure 2. Schematic drawings of the two experimental setups used to transform the upper silver stabilizer layer of HTS-tapes into silver sulfide. In both experiments, the tape samples were masked along the edges with polyimide tape to properly select the sulfurization zone and create the bCFD architecture. (a) Sulfur gel approach to form Ag_2S; (b) Sulfur sublimation approach to form Ag_2S.

Table 1. Liver of sulfur decomposition times needed for different solutions' concentrations held at different temperatures. The times marked with * indicate the samples that did present the black silver sulfide layer after being removed from the decomposed liver of sulfur solution.

XL-gel in 200 ml of water	21 °C (RT)	30 °C	35 °C	40 °C	45 °C	50 °C
0.5 ml	3 h 28 min	3 h 19 min	3 h 1 min	2 h 27 min*	1 h 11 min*	29 min*
1.0 ml	3 h 17 min	3 h 7 min	2 h 46 min	2 h 16 min*	1 h 01 min*	25 min*
1.5 ml	3 h 12 min	3 h 3 min	2 h 48 min	2 h 00 min*	48 min*	18 min*
2.0 ml	2 h 2 min	1 h 41 min	57 min	25 min	12 min	11 min

The preliminary estimation of the silver sulfide thickness was performed considering the thin film interference phenomena. As the sulfide thickness on top of silver increases from 1 to 100 nm, the color of the film changed from yellow through red-brown towards blue and, after it surpassed 100 nm, only the natural black opaque color of Ag_2S was observable [45]. In table 1, the formation of the black sulfide layer was only achieved for samples dipped in solutions with less than 2.0 ml of the XL-gel and heated to 40 °C and above. The polycrystalline cubic α-Ag_2S structure on top of the silver layer substrate was confirmed via x-ray diffraction (figure 3(b)).

All samples with a black Ag_2S layer presented blisterings (figure 3(a)) on the sulfide surface. The SEM-FIB cross-section cut in figure 4 shows the layers Ag_2S/Ag/GdBCO/MgO in the region of one of the blisters. Figures 4(b)–(d) reveal the formation of an unknown composite GdBCO + S at the Ag/GdBCO interface, followed by a structural fracture across the entire GdBCO thickness (dashed yellow line in figure 4(b)). This pattern indicates the presence of a preferential path for the liquid–solid reaction inside the structure of the silver layer.

A SEM analysis of the grown GdBCO layer (figures 5(a) and (b)) performed before the silver evaporation reveals the presence of precipitates spreading throughout the GdBCO surface. According to EDX analysis, these precipitates have the same composition as the GdBCO layer, thus allowing us to classify them as outgrowth peaks. An atomic force microscopy image of the GdBCO layer without silver suggests that these peaks cover 1% of the GdBCO's surface and can reach heights comparable to the thickness of the silver (figure S2).

Therefore, it is likely that some peaks on the surface of the GdBCO film are connected to two types of interfaces: Ag_2S/Ag and Ag/GdBCO. During the liquid sulfur reaction, the tallest peaks are the first GdBCO regions exposed to the corrosion environment of the sulfur solution, thus creating channels for infiltration all the way down to the GdBCO layer. This explanation is reinforced by the backscattered electrons image in figure 4(d), where residue pieces of degraded GdBCO are spotted in the Ag_2S layer (white regions with red contour), suggesting the presence of a GdBCO material in the silver layer even before sulfurization.

3.2. Sulfur gas reaction

Different tape samples were processed separately inside the glass jar, changing the exposure time to the sulfur gas. After

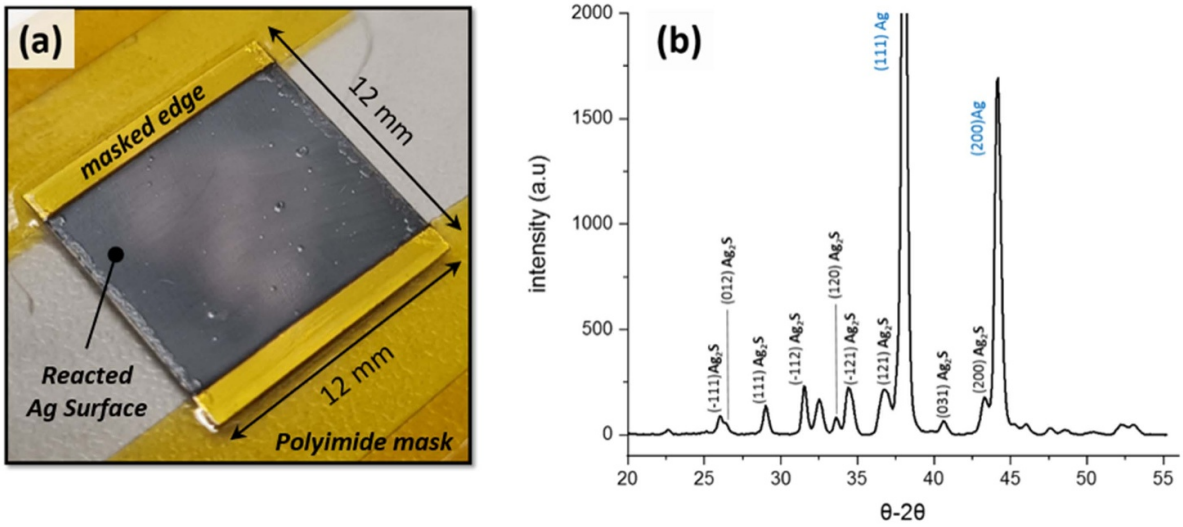

Figure 3. (a) Photo of a 12 × 12 mm tape sample attached to a glass slide and masked with polyimide tape along the edges after being submerged in the liver of sulfur solution. (b) X-ray diffraction spectra of the α-Ag_2S on top of the silver layer of a GdBCO coated conductor.

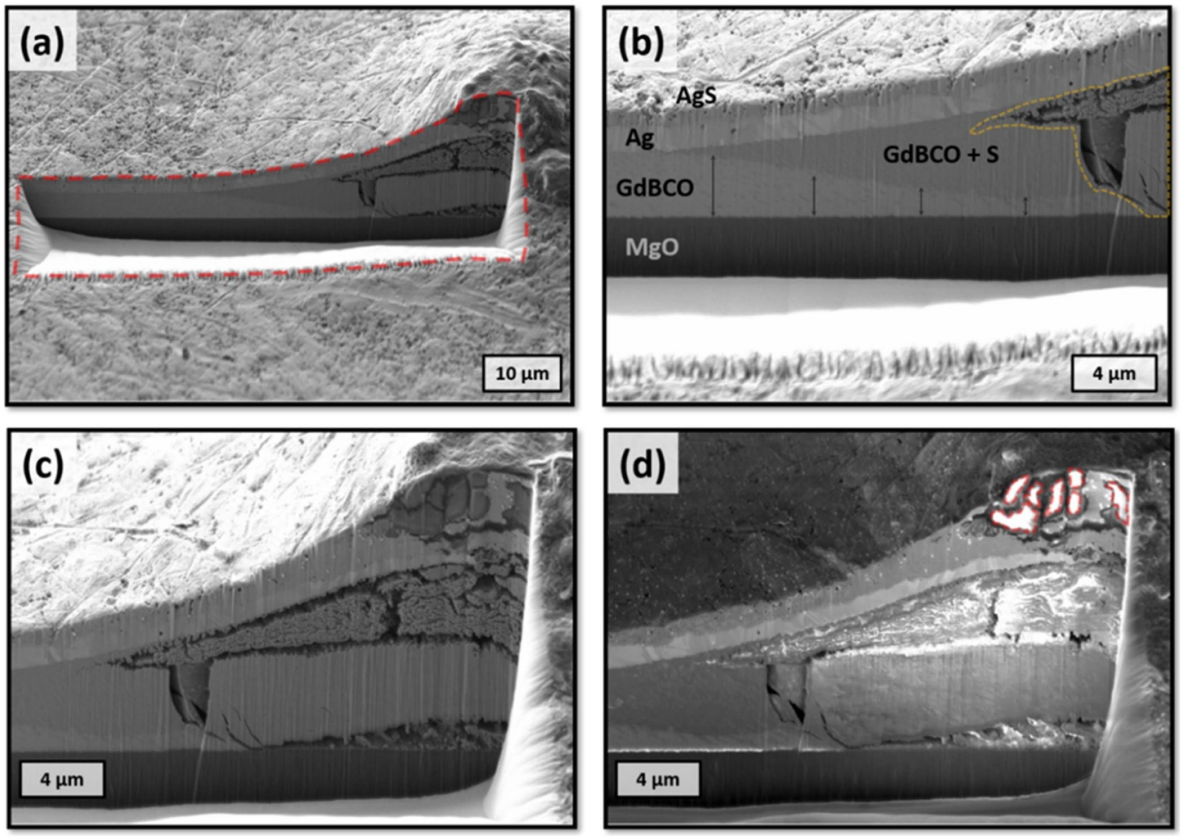

Figure 4. SEM-FIB images of the layers Ag_2S/Ag/GdBCO/MgO after the liquid sulfur reaction. (a) SE image of the cross-section cut on the side of a blister. (b) SE image showing the transition from the damaged cross-section region (GdBCO + S) to the non-damage region. (c) SE image of the center of the blister region showing damage in the Ag/GdBCO and GdBCO/MgO interfaces. (d) Backscattered electrons (BE) image of (c).

the reaction, samples were hand polished with a soft nanofiber clean cloth to remove loose Ag_2S in excess (figure 6(a)). For all samples, the surface of the Ag_2S layer presented no blistering formation after the gas reaction (figure 6(b)). The thickness of the remaining silver layer under the sulfide was measured by taking SEM images (figure 7) of the sample's cross-section after slitting trenches across the layers with a FIB.

According to the plot in figure 7, the sulfurization rate is practically linear in the first two hours of the reaction but accelerates afterward. This rate change is an indication of a change

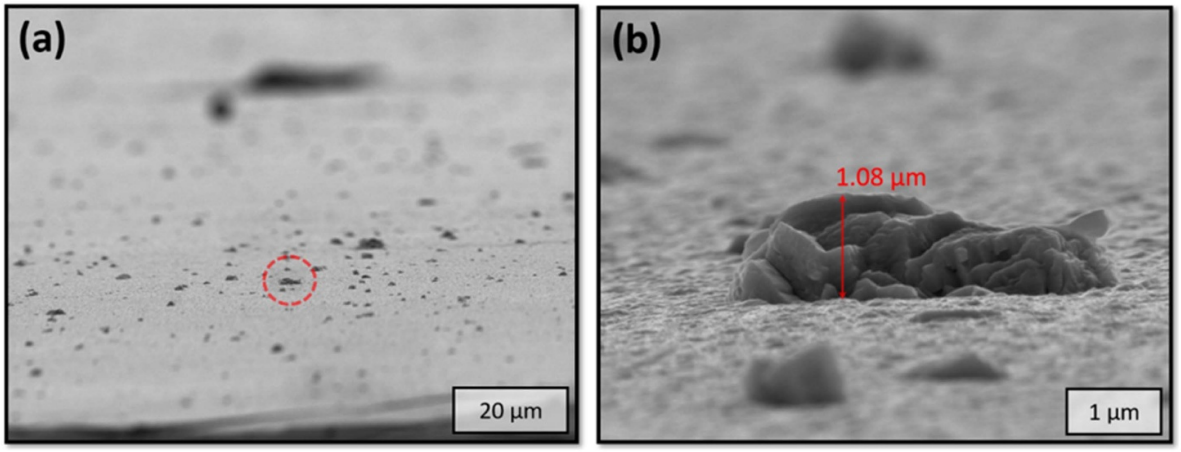

Figure 5. SEM images of the surface of a 12 × 12 mm GdBCO-tape sample tilted inside the SEM chamber. (a) Secondary electrons (SE) tilted view of the GdBCO surface, revealing the presence of many outgrowth peaks of GdBCO material. (b) Magnified SE image of one outgrowth peak achieving a height of 1 μm.

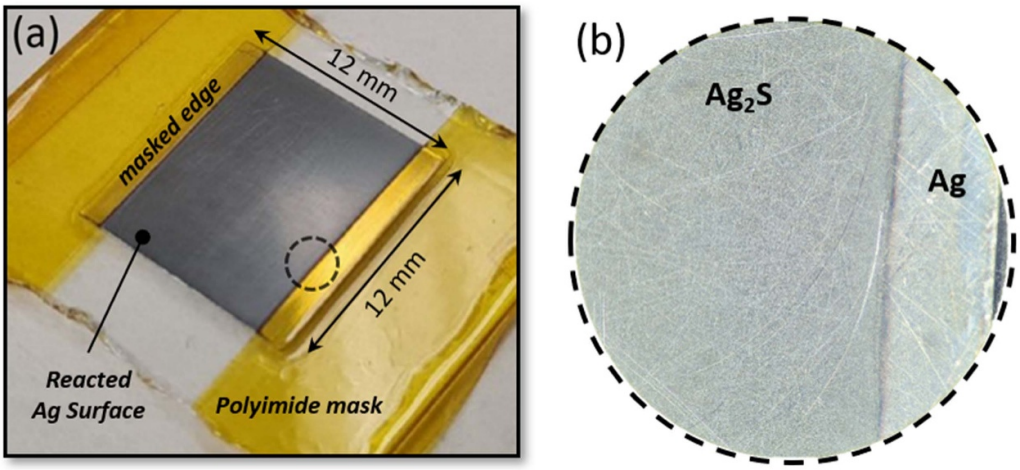

Figure 6. (a) Photo of a 12 × 12 mm tape sample stuck to a glass slide and masked with polyimide tape along the edges after the gas reaction with sulfur vapor: no sign of blistering. (b) Magnified view of the surface of the sample on the boundary between the reacted region and masked region (the polyimide tape covering the pure silver edges was removed).

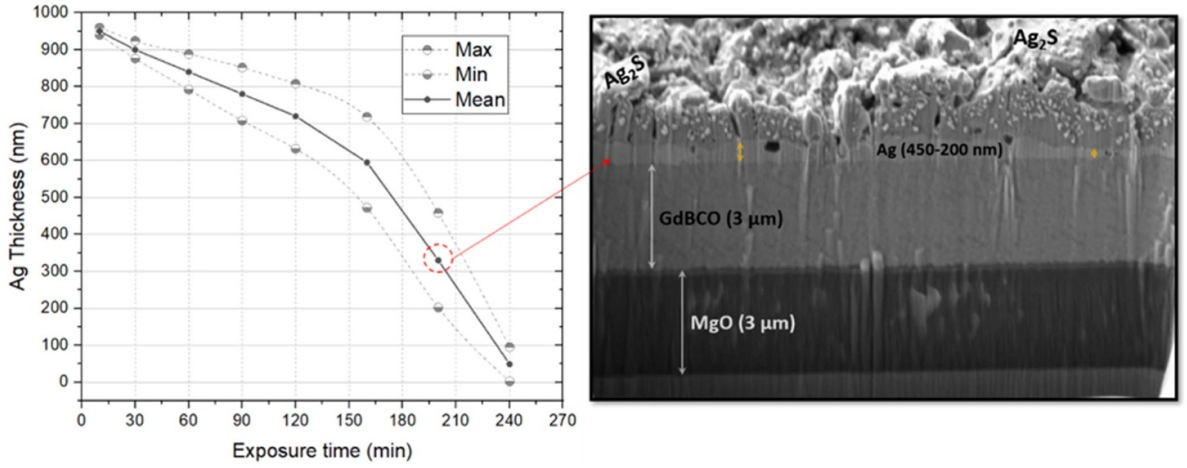

Figure 7. On the left: remaining thickness of silver after sulfurization versus exposure time to the sulfur gas. The Ag thickness was determined from SEM-FIB images and we indicate the range of film thicknesses, as determined from the images. On the right: typical SEM-FIB image of the layers Ag_2S/Ag/GdBCO/MgO after the sulfur gas reaction for 210 min.

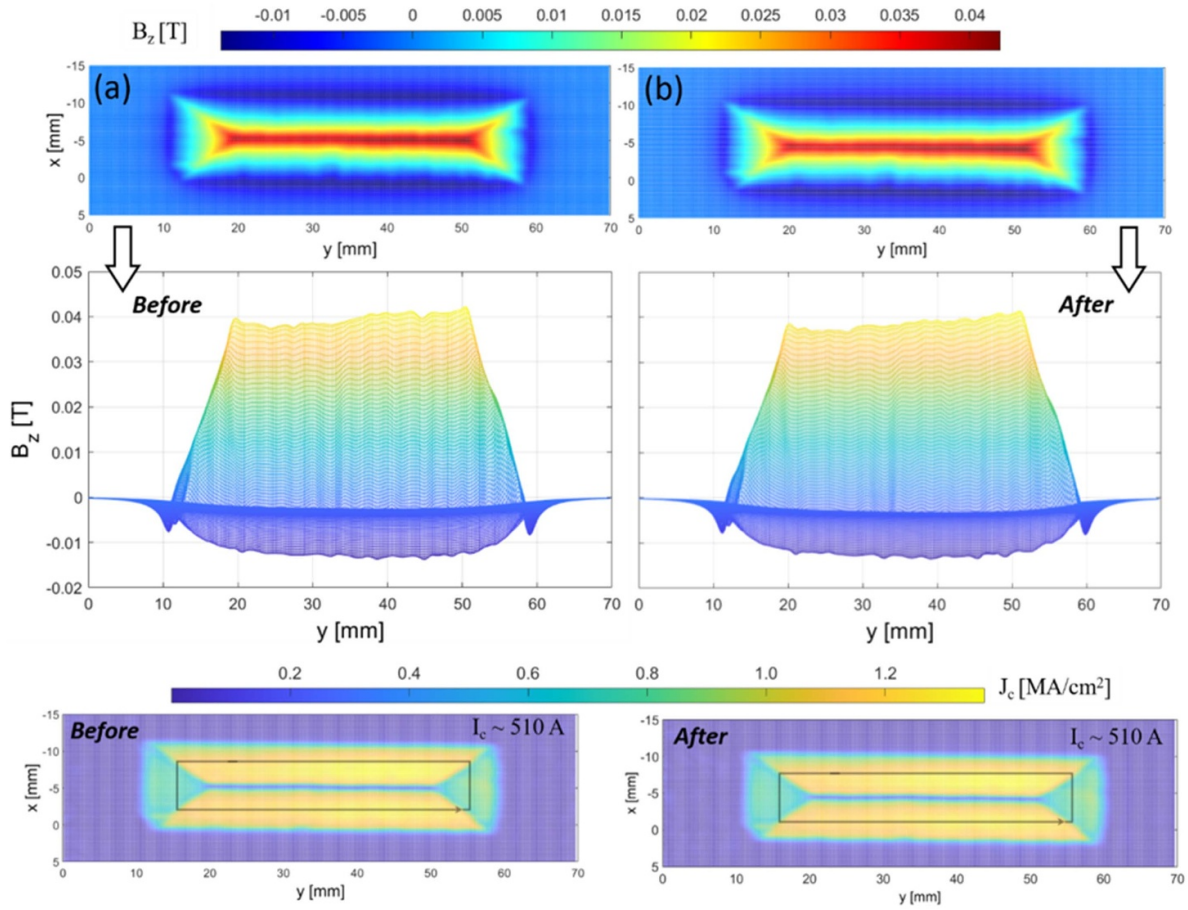

Figure 8. Perpendicular trapped field B_Z measured by scanning Hall probe microscopy (SHPM) for an HTS tape sample of 50 × 12 mm (a) before and (b) after sulfurization with S gas for 210 min. It can be concluded that there's no degradation of the superconducting properties of the GdBCO layer.

in the concentration of sulfur with time due to gas leaks and/or perhaps the formation of H_2S. Variations in the thickness of the silver layer also increases with the exposure time, reaching a maximum of 250 nm at 210 min. After four hours, the entire silver layer was consumed in the reaction, creating a flaky Ag_2S layer and leaving the GdBCO film exposed to the rich sulfur atmosphere (figure S3).

Further degradation signs were analyzed with the homemade Hall Probe microscopy system. All samples treated with exposure times less than four hours presented no detectable change, neither in amplitude nor spatially, regarding the perpendicular trapped field B_z (figure 8). This result indicates that the sulfur gas reaction, differently from the liquid-sulfur, does not take the GdBCO outgrowth peaks as a preferential path, so it avoids premature degradation of the superconducting properties of the HTS film.

3.3. DC current limitation tests

Two long samples (>12 cm) were tested in DC current limitation conditions to compare the quench behavior of a pristine unaltered sample used as reference with a sample having a bCFD architecture fabricated using the fabrication method described earlier. The samples were tested in the so-called 'hot spot' regime. The 'hot spot' regime refers to the case where the fault current level is close to the critical current of the HTS tape. In these conditions, a local normal zone is created at the location corresponding to the local minimum critical current. Considering the low normal zone propagation of commercial HTS tape, this becomes very dangerous for the integrity of the HTS tape since the current is not limited and the temperature in the local quenched zone increases drastically.

Prior to the limitation experiments, the critical current of the pristine and bCFD-sulfide samples was measured. Using a criterion of 1 μV cm^{-1}, a critical current of 285 A (n-factor of 21.5) and 267 A (n-factor of 22) at 77 K was measured for the pristine and the bCFD-sulfide sample respectively.

During the experiments, to achieve the hot spot regime, voltage pulses were successively applied by increasing the voltage level between each pulse until a local quench occurred. In figure 9, two examples of limitation tests on each sample are presented, in which a local quench was generated. In both cases, the fault current level was approximately 350 A. The voltage pulse length was chosen so the electric field generated in the sample reached approximately 14 V m^{-1}.

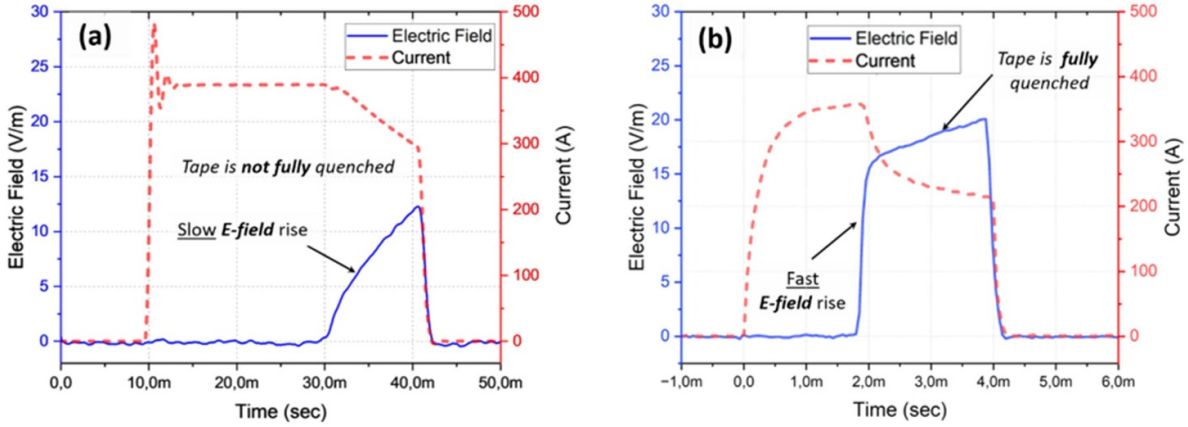

Figure 9. Electric field (V m^{-1}) and current (A) evolution during DC limitation tests in the hot spot regime for (a) a pristine THEVA tape and (b) a bCFD-sulfide tape treated for 210 min in sulfur gas.

In figure 9(a), the pristine sample took almost 10 ms to reach 14 V m^{-1} before the end of the current pulse. The rise of the electric field once a normal zone is created is 1.1–1.2 V $m^{-1}s^{-1}$ indicating a 'slow' expansion of the normal zone. Furthermore, the current slowly decreases during the rise of the electric field, which confirms that the normal zone expands very slowly.

In comparison, in figure 9(b), the bCFD-sulfide sample (treated for 210 min in sulfur gas) reached 14 V m^{-1} in less than 0.2 ms, indicating a 'rapid' expansion of the normal zone. This is confirmed from the rapid limitation of the current, reaching approximately 35% of the initial current amplitude in less than 1.7 ms. Furthermore, the rise of the electric field is approximately 60 V $m^{-1}s^{-1}$ which is 50 times higher than the pristine sample. This is consistent with NZPV measurements performed on theses samples, where it was found that the bCFD-sulfide sample had a NZPV 18 times higher than the pristine sample [15].

Note that the resistance at room temperature of the bCFD-sulfide sample was only 15% larger than the pristine sample ($\approx$0.44 Ω m^{-1}). It is therefore reasonable to assume that this difference had only a small contribution to the observed enhanced quench performance.

After the second limitation in the hot spot regime, the pristine sample presented a minor I_c degradation, from 285 to 279 A. Regarding the bCFD-sulfide sample, up to 24 limitations tests were done without seeing I_c degradation. Among the limitation tests performed, the electric field in the bCFD-sulfide sample was increased to values up to 90 V m^{-1} for pulses lasting more than 30 ms, while keeping the integrity of the sample.

4. Conclusion and outlook

Two sulfurization techniques were tested as a way to create the bCFD architecture on silver-coated GdBCO CCs. The objective was to reduce the silver thickness (1–1.2 μm) on the HTS-film side of the tape by reacting the silver with sulfur, thus creating silver sulfide, a semiconductor compound with electrical conductivity orders of magnitude lower than silver. The first attempt consisted of dipping samples into a commercial *liver of sulfur* solution, but the presence of GdBCO outgrowth peaks in the silver layer coming from the HTS-film allowed the solution to bypass the silver, and then infiltrate and degrade the GdBCO film directly. This result exemplified well why any other liquid–solid reactions on CCs metallic stabilizer should be carefully tested to avoid damaging the REBCO film due to infiltration.

In the second attempt, a gas-solid reaction was tested utilizing sulfur vapor to avoid localized reactions with the GdBCO outgrowth peaks. In vapor-pressure conditions at 130 °C, for two hours of sulfur exposure, the sulfurization rate followed a linear trend leaving variations of less than 200 nm in the silver thickness. After two hours, the reaction consumed the silver layer much faster and less homogenously, leaving variations in the silver thickness up to 250 nm. After four hours, the sulfur atmosphere consumed all the silver available and caused corrosion on the GdBCO film. This result showed that the sulfur concentration in our experiment was not ideally controlled. However, in our experimental setup, we reached the objective of partially sulfurized the silver without degrading the superconductor by exposing a tape for 3.5 h to the sulfur gas. Moreover, the expected quench performance associated with NZPV boost coming from the bCFD architecture previously demonstrated [15] was confirmed by DC limitation tests. The tests revealed that the voltage raised much faster with the bCFD-sulfide sample (60 V s^{-1}) in comparison with the pristine sample (1.2 V s^{-1}). The increase in the room temperature linear resistance (Ω m^{-1}) after sulfurization was minor (15%) and still, the tape's quench response to the hot spot regime was significantly improved. It allowed the tape to limit the current properly and avoid I_c degradation.

In conclusion, we provided a proof-of-principle of a new REBCO CC architecture based on the partial transformation of the Ag metal stabilizer into Ag_2S. The authors do not anticipate many difficulties for extending the sulfurization method to the industrial scale in a reel-to-reel process. Similar processes have already been demonstrated in the large-scale production of 2G CIGS (selenide) thin film solar cells where a continuous

flow of S or Se gas is used in the sulfurization/selenidation step (SAS). A tight control of the sulfur vapor atmosphere, temperature, and annealing time, should allow tuning the thickness of the bilayer Ag_2S/Ag, thus achieving a reliable method to commercially create the bCFD architecture which is highly promising as a new CC architecture for superconducting FCLs. In addition, this technique seems to be a simple method to be implemented in coil applications, where current sharing among the conductors should be carefully tuned based on the interlayer contact resistance between turns.

Data availability statement

The data that support the findings of this study are openly available at the following URL/DOI: www.csic.es.

Acknowledgments

The authors acknowledge the funding of this research by the FASTGRID project (EU-H2020, 721019), the projects COACHSUPENERGY (MAT2014-51778-C2-1-R), SUMATE (RTI2018-095853-BC21 and RTI2018-095853-B-C22) from the Spanish Ministry of Economy and Competitiveness which were co-funded by the European Regional Development Fund, the project 2017-SGR 753 from Generalitat de Catalunya and the COST Action NANOCOHYBRI (CA16218). ICMAB authors also acknowledge the Center of Excellence awards Severo Ochoa SEV-2015-0496 and CEX2019-000917-S.

ORCID iD

X Obradors https://orcid.org/0000-0003-4592-7718

References

[1] Obradors X and Puig T 2014 Coated conductors for power applications: materials challenges *Supercond. Sci. Technol.* **27** 044003
[2] MacManus-Driscoll J L and Wimbush S C 2021 Processing and application of high-temperature superconducting coated conductors *Nat. Rev. Mater.* **6** 587–604
[3] Awaji S, Watanabe K, Oguro H, Miyazaki H, Hanai S, Tosaka T and Ioka S 2017 First performance test of a 25 T cryogen-free superconducting magnet *Supercond. Sci. Technol.* **30** 065001
[4] Tixador P 2018 *Book: Superconducting Fault Current Limiter* vol 03 (World Scientific)
[5] Tixador P *et al* 2019 Status of the European union project FASTGRID *IEEE Trans. Appl. Supercond.* **29** 5603305
[6] Moyzykh M *et al* 2021 First Russian 220 kV superconducting fault current limiter (SFCL) for application in City Grid *IEEE Trans. Appl. Supercond.* **31** 5601707
[7] Hahn S *et al* 2019 45.5-tesla direct-current magnetic field generated with a high-temperature superconducting magnet *Nature* **570** 496–9
[8] Lao M, Bernardi J, Bauer M and Eisterer M 2015 Critical current anisotropy of GdBCO tapes grown on ISD–MgO buffered substrate *Supercond. Sci. Technol.* **28** 124002
[9] Gurevich A 2001 Thermal instability near planar defects in superconductors *Appl. Phys. Lett.* **78** 1891–3
[10] Bonura M and Senatore C 2017 Temperature and field dependence of the quench propagation velocity in industrial REBCO coated conductors *IEEE Trans. Appl. Supercond.* **27** 6600705
[11] Levin G A, Novak K A and Barnes P N 2010 The effects of superconductor–stabilizer interfacial resistance on the quench of a current-carrying coated conductor *Supercond. Sci. Technol.* **23** 014021
[12] Bonura M and Senatore C 2016 An equation for the quench propagation velocity valid for high field magnet use of REBCO coated conductors *Appl. Phys. Lett.* **108** 242602
[13] Van Nugteren J, Dhallé M, Wessel S, Krooshoop E, Nijhuis A and Ten Kate H 2015 Measurement and analysis of normal zone propagation in a ReBCO coated conductor at temperatures below 50 K *Phys. Proc.* **67** 945–51
[14] Kudymow A, Noe M, Schacherer C, Kinder H and Prusseit W 2007 Investigation of YBCO coated conductor for application in resistive superconducting fault current limiters *IEEE Trans. Appl. Supercond.* **17** 3499–502
[15] Lacroix C *et al* 2022 Normal zone propagation in various REBCO tape architectures *Supercond. Sci. Technol.* **35** 055009
[16] Diko P, Piovarči S, Antal V, Kaňuchová M and Volochová D 2018 Corrosion of YBCO bulk superconductor in air *J. Am. Ceram. Soc.* **101** 3703–9
[17] Ekin J 2006 *Experimental Techniques for Low-Temperature Measurements* (Oxford University PressOxford)
[18] Fu Y, Tsukamoto O and Furuse M 2003 Copper stabilization of YBCO coated conductor for quench protection *IEEE Trans. Appl. Supercond.* **13** 1780–3
[19] Tixador P and Nguyen N T 2012 Design of ReBaCuO-coated conductors for FCL *Supercond. Sci. Technol.* **25** 014009
[20] Wang X, Trociewitz U P and Schwartz J 2009 Self-field quench behaviour of $YBa_2Cu_3O_{7-\delta}$ coated conductors with different stabilizers *Supercond. Sci. Technol.* **22** 085005
[21] Lacroix C, Lapierre Y, Coulombe J and Sirois F 2014 High normal zone propagation velocity in second generation high-temperature superconductor coated conductors with a current flow diverter architecture *Supercond. Sci. Technol.* **27** 055013
[22] Lacroix C, Sirois F and Wertheimer M R 2015 Patent US20150045231—increased normal zone propagation velocity in superconducting segments
[23] Lacroix C and Sirois F 2014 Corrigendum: concept of a current flow diverter for accelerating the normal zone propagation velocity in 2G HTS coated conductors *Supercond. Sci. Technol.* **27** 129501
[24] Lee J-H, Lee H, Lee J-W, Choi S-M, Yoo S-I and Moon S-H 2014 RCE-DR, a novel process for coated conductor fabrication with high performance *Supercond. Sci. Technol.* **27** 044018
[25] Fournier-Lupien J H, Lacroix C, Huh J, Masse J P, Bellemare J and Sirois F 2021 Effect of annealing on HTS tapes with a cerium oxide layer inserted between the REBaCuO and silver layers *Materialia* **15** 101029
[26] Barusco P *et al* 2022 Chemical solution deposition of insulating yttria nanolayers as current flow diverter in superconducting $GdBa_2Cu_3O_{7-\delta}$ coated conductors *ACS Omega* **7** 15315–25
[27] Lacroix C, Sirois F and Lupien J-H F 2017 Engineering of second generation HTS coated conductor architecture to enhance the normal zone propagation velocity in various operating conditions *Supercond. Sci. Technol.* **30** 064004
[28] Fournier-Lupien J-H, Lacroix C, Hellmann S, Huh J, Pfeiffer K and Sirois F 2018 Use of the buffer layers as a current flow diverter in 2G HTS coated conductors *Supercond. Sci. Technol.* **31** 125019

[29] Nelson A J, Asher S E, Beall J A and Moreland J 1991 Morphology of silver on $YBa_2Cu_3O_{7-\delta}$ thin films *IEEE Trans. Magn.* **27** 1616–8
[30] Ikuma Y and Akiyoshi S 1998 Diffusion of oxygen in $YBa_2Cu_3O_{7-y}$ *J. Appl. Phys.* **64** 3915
[31] Kim H S, Song J B, Kwon N Y, Kim K L and Lee H G 2009 The influence of heat-treatment and oxygenation annealing on the superconducting properties of YBCO coated conductors *Supercond. Sci. Technol.* **22** 125016
[32] Cayado P, Sánchez-Valdés C F, Stangl A, Coll M, Roura P, Palau A, Puig T and Obradors X 2017 Untangling surface oxygen exchange effects in $YBa_2Cu_3O_{6+x}$ thin films by electrical conductivity relaxation *Phys. Chem. Chem. Phys.* **19** 14129–40
[33] Stangl A 2019 Oxygen kinetics and charge doping for high critical current YBCO films *PhD Thesis* Universitat Autònoma de Barcelona
[34] Stanbery B J, Abou-Ras D, Yamada A and Mansfield L 2022 CIGS photovoltaics: reviewing an evolving paradigm *J. Appl. Phys.* **55** 173001
[35] Lokhande A C, Chalapathy R B V, He M, Jo E, Gang M, Pawar S A, Lokhande C D and Kim J H 2016 Development of Cu_2SnS_3 (CTS) thin film solar cells by physical techniques: a status review *Sol. Energy Mater. Sol. Cells* **153** 84–107
[36] López-García J *et al* 2015 Synthesis of $CuIn(S,Se)_2$ quaternary alloys by screen printing and selenization-sulfurization sequential steps: development of composition graded absorbers for low cost photovoltaic devices *Mater. Chem. Phys.* **160** 237–43
[37] Prusseit W, Nemetschek R, Hoffmann C, Sigl G, Lümkemann A and Kinder H 2005 ISD process development for coated conductors *Physica* C **426–431** 866–71
[38] Bauer M, Metzger R, Semerad R, Berberich P and Kinder H 1999 Inclined substrate deposition by evaporation of magnesium oxide for coated conductors *MRS Proc.* **585** 35–44
[39] Metzger R, Bauer M, Numssen K, Semerad R, Berberich P and Kinder H 2001 Superconducting tapes using ISD buffer layers produced by evaporation of MgO or reactive evaporation of magnesium *IEEE Trans. Appl. Supercond.* **11** 2826–9
[40] Oh S S, Kim H S, Ha H S, Ko R K, Ha D W, Lee H, Moon S H and Yoo S I 2013 Progress in research and development for REBCO coated conductors by reactive co-evaporation *Prog. Supercond. Cryog.* **15** 1229–3008
[41] Anon 1921 *Platers' Guide: With Which is Combined Brass World* (Brass World Publishing Company, Incorporated)
[42] Lyons J R 2008 An estimate of the equilibrium speciation of sulfur vapor over solid sulfur and implications for planetary atmospheres *J. Sulfur Chem.* **29** 269–79
[43] Granados X, Iliescu S, Bozzo B, Bartolome E, Puig T, Obradors X, Amorós J and Carrera M 2006 Magnetic mapping—a way to test and understand current flows in thin and bulk superconductors *Adv. Sci. Technol.* **47** 1–6
[44] Lacroix C *et al* 2021 Successful DC current limitation above 100 Vm −1 for 50 ms using HTS tapes with critical currents exceeding 750 A/cm-width *Supercond. Sci. Technol.* **34** 025015
[45] Selwyn L 2004 *Metals and Corrosion: A Handbook for the Conservation Professional* (Canadian Conservation Institute)